Computers and Geotechnics 139 (2021) 104386

Contents lists available at ScienceDirect

Computers and Geotechnics

journal homepage: www.elsevier.com/locate/compgeo

Research paper

Investigation of soil–pile–structure interaction induced by vertical loads and tunnelling

A. Franza [a,*], C. Zheng [b], A.M. Marshall [c], R. Jimenez [b]

[a] Department of Civil and Architectural Engineering, Aarhus University, Aarhus, Denmark
[b] ETSI Caminos, Universidad Politécnica de Madrid, Madrid, Spain
[c] Department of Civil Engineering, University of Nottingham, Nottingham, UK

ARTICLE INFO

Keywords:
Piles
Tunnelling
Soil-structure-interaction
Building
Deformations

ABSTRACT

The response of pile groups and piled structures to vertical and tunnelling-induced loads is studied. A two-stage model is adopted that can efficiently consider external actions, greenfield tunnelling movements, superstructure stiffness, ultimate pile shaft and base stresses, pile-soil interactions in uniform or layered soils, and local soil behaviour (as either linear elastic, elastic perfectly-plastic, or nonlinear). Several scenarios are analysed: namely, piles subjected to vertical loads; piles and piled structures that are affected by tunnelling induced ground movements. Model results for piles under vertical loads compare well with field and other analytical models, confirming the robustness of the model. For tunnelling adjacent to or beneath single piles and pile groups, the impact of layered soils, soil yielding, and hyperbolic transfer mechanisms are shown to be significant, indicating that these aspects should be considered in risk assessments when using simplified models. Analyses of tunnelling beneath free-head piles and piled equivalent beams (describing flexible slabs or stiff buildings) confirm that pile-foundation connections and superstructures decrease tunnelling-induced displacements and deformations at the surface level; however, their action can also worsen the foundation distress with respect to force-moment structural capacity. Considering that the envelopes of fully-flexible and perfectly rigid superstructures will not always be conservative, soil-pile-structure interaction models are recommended for design.

1. Introduction

The behaviour of piles under static loading has been a subject of practical research for several decades. To overcome empiricism and conservatism in preliminary design, engineers need reliable prediction models to estimate pile group displacements induced by external actions and superstructure live loads, referred to as *active loads*. In addition, engineers also need methods to predict the effect of *passive loads* on pile foundations which are caused by ground movements resulting from excavations. For both scenarios, the problem is characterised by pile-soil-pile and pile-structure interactions. Therefore, soil-foundation-structure interaction prediction models should be developed for practical analysis and design purposes.

Performance-based design methods have driven the need for more accurate prediction methods for foundations under serviceability conditions of vertical loads. This has arguably been one of the main driving factors for incorporating more costly numerical analyses (e.g., finite elements) within routine design. However, as demonstrated by Sheil et al. (2019), simplified models that incorporate soil plasticity and stiffness degradation at the pile-soil interface, while still assuming an elastic interaction between piles, can provide computationally efficient results that compare well with advanced numerical models and field data.

For active vertical loads, simplified analysis methods are classified herein depending on how they describe the local and interaction aspects of the soil-foundation behaviour. For pile-soil interaction (PSI), the following models are available: the continuum approach, modelling the 3D soil response to multi-directional loading at the soil-pile interface using half-space theory (Poulos, 1989; Basile, 1999; Cairo and Conte, 2006); the Winkler approach, considering a decoupled soil response to uni-directional loads (Chow, 1986; Lee and Xiao, 2001; Zhang et al., 2016); and the lumped single degree of freedom (DOF) approach, describing the overall pile stiffness to the pile head loads (Mandolini and Viggiani, 1997). For pile-soil-pile interaction (PPI), the following models are available: the continuum interaction factor approach, in which the soil flexibility considers the interaction between all DOFs (Poulos, 1989; Basile, 1999; Xu and Poulos, 2001);

* Corresponding author.
E-mail address: anfr@cae.au.dk (A. Franza).

https://doi.org/10.1016/j.compgeo.2021.104386
Received 17 March 2021; Received in revised form 12 July 2021; Accepted 29 July 2021
Available online 2 September 2021
0266-352X/© 2021 The Authors. Published by Elsevier Ltd. This is an open access article under the CC BY license (http://creativecommons.org/licenses/by/4.0/).

Notation

c	Rebar cover
d_p	Pile diameter
f	Local soil reaction force
f_{cd}	Concrete design strength
f_{yd}	Steel design strength
f_f	Ultimate soil force
$f_{f,i,down}$	Limit force in relative down-drag
$f_{f,i,up}$	Limit force in relative uplift
ν_s	Poisson's ratio for soil
q_f	Base ultimate stress
ρ	Steel reinforcement percentage
s_p	Pile spacing
τ	Shaft stress
τ_f	Shaft ultimate stress
u_x	Horizontal displacement
u_z	Vertical displacement
z	Depth, measured from ground surface
z_t	Depth of tunnel axis
A_p	Pile cross-sectional area
E_p	Young's modulus of pile
E_s	Young's modulus of soil
$E_{s,0}$	Initial Young's modulus of soil
$E_{s,0}^{L,i}$	Initial Young's modulus of the ith soil layer
K	Coefficient of horizontal pressure
L_p	Pile length
M	Pile bending moment
N	Pile axial force
P_0	Pre-tunnelling service load at the pile head
Q_t	Maximum capacity of pile
R	Tunnel radius
R_f	Coefficient of hyperbolic stiffness reduction
SF_0	Initial safety factor
$V_{l,t}$	Volume loss of tunnel
X_{cap}	Cap offset
$\mathbf{f}$	Vector of forces acting on the soil
$\mathbf{p}$	External loading vector
$\mathbf{u}$	Pile displacement vector
$\mathbf{u}^{ip}$	Slider displacement vector
$\mathbf{u}^{cat}$	Greenfield ground displacement vector
$\mathbf{R}$	Near-pile stiffness reduction matrix
$\mathbf{S}$	Structure stiffness matrix
$\mathbf{L}$	Elastic soil flexibility matrix
$\mathbf{L}^*$	Non-diagonal term of $\mathbf{L}$
$\mathbf{K}^*$	Soil near-pile stiffness matrix
GF	Greenfield
EL	Elastic solution
EP	Elastoplastic solution
NL	Nonlinear solution
NP	Nonlinear elastoplastic solution
RC	Reinforced concrete
UC	Unreinforced concrete

the Winkler logarithmic attenuation function that limits the interaction between piles to DOFs at a specific depth (Randolph and Wroth, 1979; Lee and Xiao, 2001; Zhang et al., 2016); and the lumped factors approach, describing pile to pile interaction with a scalar (Cairo and Conte, 2006; Zhang et al., 2010). Finally, for the local soil-pile interface response, elastic perfectly-plastic (Basile, 1999; Leung et al., 2010; Stutz et al., 2014; Franza and Sheil, 2021), trilinear (Liu et al., 2004; Dias and Bezuijen, 2018b), and hyperbolic (Chow, 1986; Mandolini and Viggiani, 1997; Zhang et al., 2016) behaviour have been implemented. In this paper, the *continuum approach* based on elasticity theory is adopted for both PSI and PPI, while various interface behaviours are considered.

When a new tunnel is excavated below the pile tip level (*tunnelling beneath piles*), there is potential for large pile settlements and differential movements between piles (Bel et al., 2016; Hong et al., 2015; Marshall and Mair, 2011; Williamson et al., 2017) that can lead to foundation tilt (Soomro et al., 2015; Ng et al., 2014; Yoo, 2013) and to superstructure distortions (Franza and Marshall, 2018). When the tunnel axis is above the pile tip level (*tunnelling adjacent to piles*), pile deflection and negative friction characterise the response of piles with bending moments close to the tunnel shoulder and at pile-cap connections (Basile, 2014; Loganathan et al., 2001; Ng et al., 2014). A dimensionless framework was proposed by Korff et al. (2016), and extended by Franza et al. (2021), to estimate settlements and internal forces of isolated piles subjected to ground settlements; this extended approach considers the influence of the settlement magnitude and the initial pile safety factor $SF_0 = Q_t/P_0$, where Q_t is the pile capacity and P_0 the pile head load prior to the excavation. This framework attempts to overcome some limitations of empirical methods for predicting excavation induced pile settlements (e.g., Selemetas and Standing, 2017). However, the assessment of foundation structural damage depends on the axial and flexural response of the pile, requiring an interaction model for accurate prediction.

Several aspects of this problem require further investigation. Experimental evidence has confirmed that the pile safety factor alters the tunnel-soil-pile interaction (Williamson et al., 2017; Marshall et al., 2020), while centrifuge tests have also highlighted the coupled effects of superstructure stiffness and buildings self-weight (Franza and Marshall, 2018; Song and Marshall, 2020). However, linear elastic models cannot describe the influence of a pile's loading conditions (i.e. initial safety factor). Therefore, more complex near-pile soil behaviour, to model the load transfer mechanisms between the pile and the soil, should be considered. Although elastic perfectly-plastic (Basile, 2014), hyperbolic (Korff et al., 2016), and tri-linear (Dias and Bezuijen, 2018a) load-transfer mechanisms have been used for isolated piles affected by tunnelling, continuum-based models of pile groups considering pile-to-pile interaction (in which the soil stiffness matrix is obtained from half-space theory, as opposed to approximated Winkler models) are mostly limited to linear elastic soil behaviour (Loganathan et al., 2001; Xu and Poulos, 2001), particularly for layered grounds (Huang and Mu, 2012; Mu et al., 2012). In fact, the use of nonlinear load transfer mechanisms in continuum-based models of multiple piles is limited to elastic-perfectly plastic behaviour (Basile, 2014). On the other hand, attempts to consider the influence of the superstructure stiffness are limited to linear elastic Winkler soil models (Franza et al., 2017). For pile groups, previous research focused on tunnelling adjacent to piles with free-heads and a rigid elevated cap (Loganathan et al., 2001; Basile, 2014); however, the impact of soil nonlinearities for tunnelling beneath capped pile groups is unclear.

This paper aims at exploring the nonlinear response of pile groups and piled structures to external (*active*) and tunnelling-induced (*passive*) loads using a proposed two-stage model named COMPILE, which is designed for practical use due to its computational efficiency. This model, implemented as a MATLAB code, conducts a *fully coupled* analysis of the soil-foundation-structure system, considering both yielding and hyperbolic local stiffness degradation of the soil. The new model extends the work of Franza et al. (2021) (which was limited to single piles in uniform ground) to layered ground and, additionally, integrates these improvements into the models from Franza et al. (2017, 2019) (which were limited to a linear elastic model of pile groups and piled structures in uniform soil). By combining the modelling capabilities

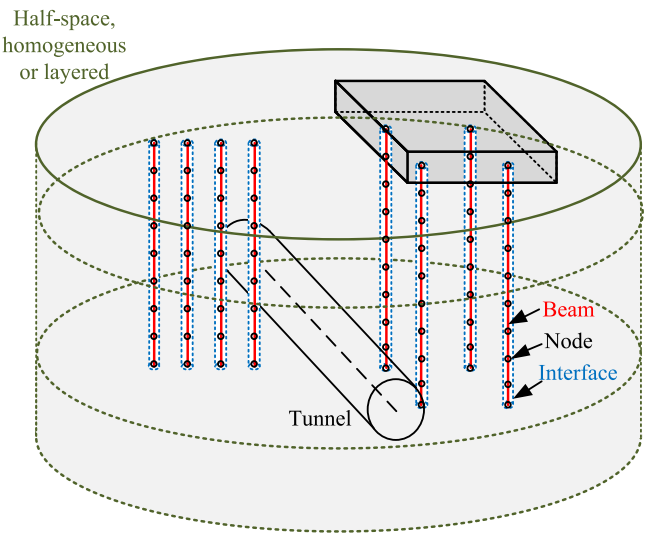

Fig. 1. Sketch of the mechanical model.

from these previous studies into the COMPILE model, it is possible to achieve greater fidelity in the description of the interaction problem, while obtaining a versatile and efficient model for preliminary design. Both pile displacements and internal forces can be estimated. In the context of tunnelling, results illustrate that neglecting the structure influence (for both flexible slabs and stiff structures) on the foundation distress can be unconservative and, thus, that pile-soil-structure interaction analyses should be preferred to single pile assessments when possible.

2. Scope

The COMPILE nonlinear model is presented here to better characterise the response to active and passive loads of pile groups and piled structures in homogeneous or layered ground. In particular, post-tunnelling forces and displacements of the piles are studied.

3. Model

The COMPILE mechanical model is illustrated by Fig. 1. A group of vertical piles of length L_p, diameter d_p, and Young's modulus E_p is considered. Piles are modelled as Euler-Bernoulli beam elements. The superstructure, connected to the pile heads by tie constraints, is assumed to be linear elastic and is modelled using a condensed stiffness matrix. Any superstructure may be implemented; in this paper, for simplicity, (nearly) rigid caps or an equivalent beam are considered. The soil is modelled as either a homogeneous or layered half-space (referred to as a *continuum*), characterised by the initial Young's modulus $E_{s,0}$ and Poisson's ratio ν_s for each layer. Soil nonlinearity (i.e. soil stiffness degradation) and plasticity (i.e. soil yielding, or limit shaft or base stress) is limited to the area near the pile shaft and base (referred to as *near-pile*) and it is modelled by a perfectly plastic linear/nonlinear interface, while the interactions between nodes along a given pile and between different piles (referred to as *far-pile*) are assumed to be linear elastic (Chow, 1986). The soil flexibility matrix, describing the continuum (i.e. elastic half-space) displacements due to vertical and horizontal load distributions along the piles' axes, is obtained by integrating along the pile boundary the elastic solutions of Mindlin (1936) and Ai et al. (2002) for the homogeneous and layered ground cases, respectively.

The near-pile soil response, describing the local relationship between ground forces and displacements at a given node, is considered either (i) fully linear elastic (EL solution), (ii) linear elastic perfectly plastic (EP solution, see Fig. 2a), or (iii) nonlinear elastoplastic (NP solution, see Figs. 2b and c), whereas the far-pile behaviour, describing the relationship between ground nodal forces and displacements at other nodes, is assumed linear elastic and characterised by the initial stiffness $E_{s,0}$. For the EP solution, sliders placed at the pile-soil interface provide the near-pile perfectly-plastic response. For the NP solution, in addition to the sliders, the near-pile tangent Young's modulus E_s was adjusted by modifying the diagonal terms of the soil flexibility matrix to consider its dependency on the loading path (e.g. loading and unloading) and its degradation with deformations, as displayed by Fig. 2b. For loading and reverse loading, the tangent Young's modulus of the near-pile soil E_s is given by $E_s = E_{s,0} \times \left(1 - R_f \times f/f_f\right)^2$, which depends on the ratio between the local soil reaction forces f and their ultimate values f_f, and on the coefficient of hyperbolic stiffness reduction R_f (Castelli and Maugeri, 2002; Chow, 1986; Basile, 2014). For unloading-reloading, the local stiffness is assumed equal to the initial Young's modulus $E_{s,0}$. Finally, the EP and NP behaviours were only implemented in the vertical direction, whereas a linear elastic response (EL) was considered in the horizontal direction (Basile, 2014).

As in other two-stage approaches (Basile, 2014; Loganathan et al., 2001), tunnelling is modelled using an input of greenfield ground movements while the continuum response to loading is not affected by the presence of the tunnel. In this paper, the semi-analytical formulas proposed by Loganathan and Poulos (1998) were adopted for greenfield soil displacements to allow for comparison with previous studies that used the same greenfield input; however any field, empirical, or numerically derived input for greenfield displacements may be used.

The two-stage approach is implemented as follows. In Stage 1, the external and live loads are applied to the pile heads, cap, or superstructure; then, the full system (including soil, foundation, and superstructure) is solved to obtain the *pre-tunnelling* results. For tunnelling, this is followed by Stage 2, in which the full system is subjected to the tunnelling-induced passive loads generated by the greenfield movements. At the end of Stage 2, the *post-tunnelling* foundation conditions (displacements and internal forces) are evaluated. *Tunnelling-induced* displacements and internal forces are inferred from the variation between Stages 1 and 2. Numerically, the Finite Element Method (FEM) model was obtained by solving Eqs. (1)-(3), where Eq. (1) is the equilibrium equation; Eq. (2) describes the near-pile stiffness; and Eq. (3) accounts for the sliders. The fully linear elastic solution (EL) is obtained from Eqs. (1) and (2) using $R_f = 0$; the elastic perfectly-plastic solution (EP) is obtained from Eqs. (1)-(3) imposing $R_f = 0$; and the nonlinear elastoplastic solution (NP) is given by Eqs. (1)-(3) for $R_f \neq 0$. In this paper, $R_f = 1$ is considered for NP analyses, unless otherwise indicated. The equations are:

$$\begin{aligned} &(\mathbf{S} + \mathbf{K}^*)\,\mathbf{u} = \mathbf{p} + \mathbf{K}^*\mathbf{u}^{cat} + \mathbf{K}^*\mathbf{L}^*\langle\mathbf{f}\rangle + \mathbf{K}^*\mathbf{u}^{ip}; \\ &\mathbf{f} = (\mathbf{p} - \mathbf{S}\mathbf{u}); \qquad \mathbf{K}^* = \mathbf{R}\,(\mathbf{L} - \mathbf{L}^*)^{-1} \end{aligned} \tag{1}$$

$$R_{ii} = \begin{cases} 1, & \text{for unloading} \\ \left(1 - R_f \dfrac{f_i}{f_{f,i,down}}\right)^2, & \text{for loading} \\ \left(1 - R_f \dfrac{f_i}{f_{f,i,up}}\right)^2, & \text{for reverse loading} \end{cases} \tag{2}$$

$$\langle\mathbf{f}\rangle_i = f_{f,i,up} < (\mathbf{p} - \mathbf{S}\mathbf{u})_i < f_{f,i,down} \tag{3}$$

where $\mathbf{u}$ is the displacement vector of nodes along the pile foundation (consisting of three translational and three rotational DOFs), $\mathbf{p}$ is the external loading vector (defined with respect to all nodes, but having nonzero elements only at the pile heads which represent the load transmitted by the superstructure), $\mathbf{f}$ is the vector of forces applied by the foundation nodes to the soil (i.e. a vector containing the forces acting on the soil medium), $\mathbf{S}$ is the stiffness matrix of the structure (consisting of both the pile foundation and the condensed superstructure stiffness matrix), $\mathbf{u}^{ip}$ is the plastic slider displacement vector, $\mathbf{u}^{cat}$ is the greenfield ground displacement vector, $\mathbf{L}$ is the linear elastic

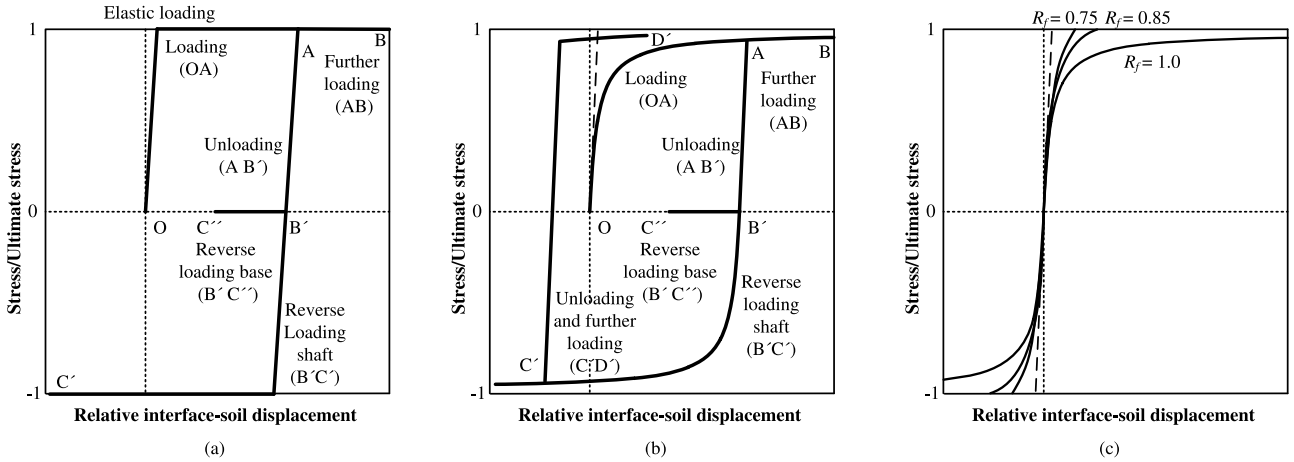

Fig. 2. Near-pile soil behaviour: (a) linear elastic perfectly plastic (EP); (b) nonlinear elastoplastic (NP) (Franza et al., 2021) (follow the letter order for loading paths); (c) influence of coefficient R_f of hyperbolic stiffness reduction.

soil flexibility matrix relating the soil displacement field to the point of application of a force, $\mathbf{L}^*$ is the non-diagonal term of $\mathbf{L}$ (i.e. the soil flexibility matrix without the main diagonal), and $\mathbf{K}^*$ is the local (near-pile) stiffness matrix of the soil (i.e. for no stiffness degradation, it is the inverse matrix of the diagonal term of $\mathbf{L}$ for the linear elastic behaviour in the near-pile soil). The terms $f_{f,i,up}$ (negative) and $f_{f,i,down}$ (positive) are the nodal limit forces for pile uplift and down-drag relative to the soil, which are given by the integration of the ultimate base, q_f, and shaft, τ_f, stresses while no tensile capacity is considered at the pile base. $\mathbf{R}$ is the near-pile stiffness reduction matrix, resulting in the initial linear elastic stiffness during unloading and hyperbolic stiffness degradation for loading and reverse loading. The EL equations can be solved directly, whereas the EP and NP solutions require an incremental and iterative procedure (for both Stages 1 and 2).

4. Nonlinear pile response to vertical loads

Two ideal foundations with single piles are analysed first to validate the new COMPILE model against continuum-based elastic perfectly plastic results from Basile (1999) and Poulos (1989). The "Supplemental Materials" report the load-settlement results from the COMPILE model and demonstrate the excellent agreement with the other models, and particularly with the results of Poulos (1989) who used a similar approach for the soil flexibility.

Next, predictions are compared against field loading test data from O'Neill et al. (1982) for a single pile and for groups of 2 × 2 and 3 × 3 piles in stiff over-consolidated clay. For comparison, the predictions of Castelli and Maugeri (2002), Zhang et al. (2016), and Chow (1986), obtained using simplified models, are also reported. In the field, the piles consisted of closed-end steel pipes (diameter d_p = 274 mm, wall thickness 9.3 mm, and axial stiffness E_pA_p = 1.6 GN) with a length L_p = 13.1 m. Pile groups were capped by a rigid concrete block and had their centres spaced at $3d_p$. The ground was characterised by a linearly increasing undrained shear strength, while the Poisson's ratio was assumed as 0.5. As reported by Chow (1986), the soil shear modulus inferred from soil cross-hole test data indicated a Young's modulus varying between E_s = 144 MPa and 453 MPa along the pile shaft, τ_f = 16.2 kPa and 81.2 kPa at the top and bottom of the shaft (considering a reduction factor α = 0.34), and q_f = 2.15 MPa. In our analyses, these soil properties were adopted, along with an average E_s = 300 MPa; additionally, varying conditions of the near-pile soil behaviour were considered according to the adopted hyperbolic coefficient: perfectly-plastic EP analysis (R_f = 0), nonlinear NP analysis (R_f = 1), and nonlinear plastic NP analysis (R_f = 0.9) (refer to Fig. 2).

Fig. 3a compares the COMPILE results against the single pile field data. The model gives a good prediction of the initial response as well

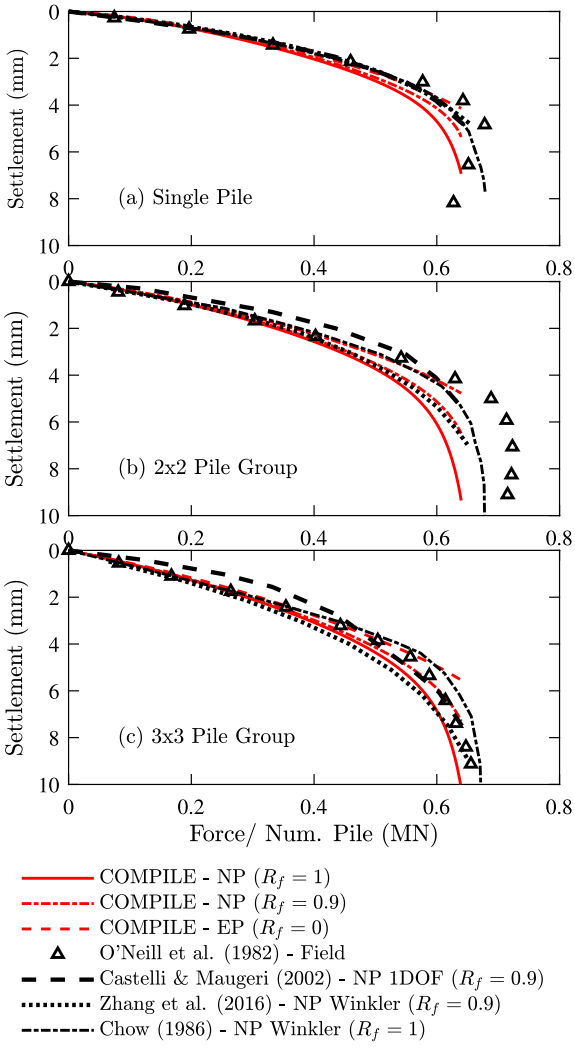

Fig. 3. Measured and calculated load-settlement curves at pile head of the (a) single pile, (b) 2 × 2 and (c) 3 × 3 pile group.

as the stiffness degradation up to an intermediate settlement of about 4 mm (1.5%d_p). The purely hyperbolic near-pile soil model (R_f = 1)

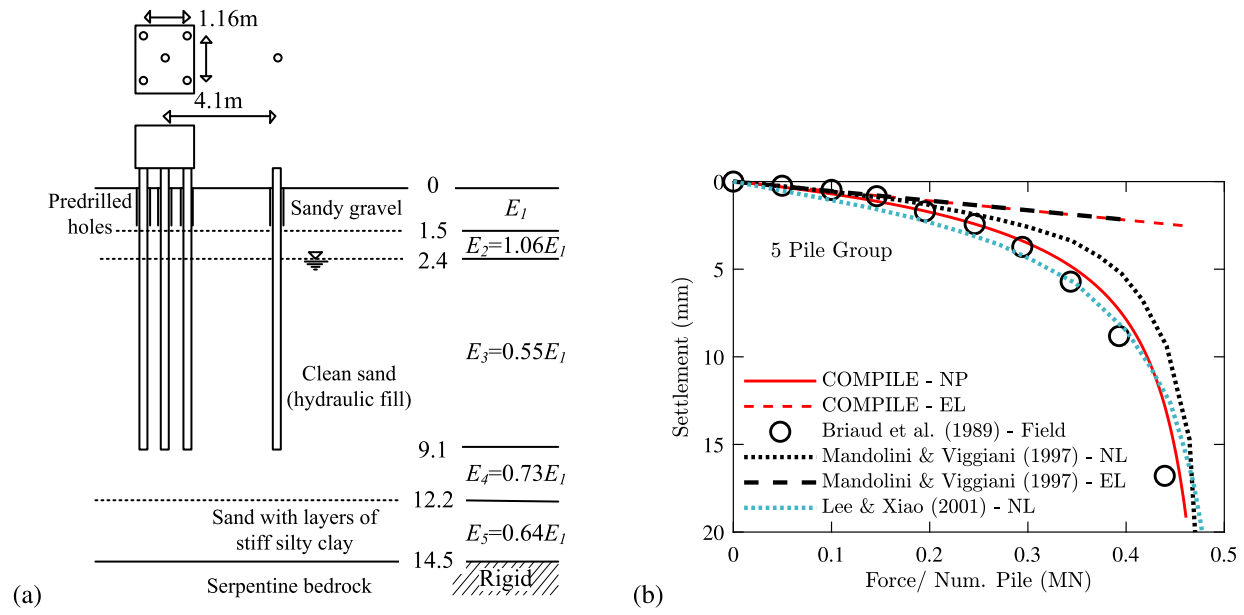

Fig. 4. (a) Layout of the field test and ground model (Mandolini and Viggiani, 1997); (b) measured and calculated load-settlement curves at the pile head of the 5-pile group.

overestimates the stiffness degradation, whereas the NP model with $R_f = 0.9$ (the value adopted in other nonlinear simplified analyses; see Castelli and Maugeri (2002)) matches better the field measurements. For pile group results in Fig. 3b and c, the simplified model results show greater variability; however, in general, COMPILE's results agree well with those of the other simplified solutions and with the field data, especially for the 3 × 3 pile group. For the 2 × 2 pile group, stiffness degradation is over-predicted by all the models considered at settlements greater than 6 mm.

Finally, results for a layered ground scenario are presented. Briaud et al. (1989) tested a single pile and a 5-pile group driven in granular soil in San Francisco (see Fig. 4a). The piles were closed-end steel pipes (diameter $d_p = 273$ mm, wall thickness 9.3 mm, $E_pA_p = 1.58$ GN) embedded 9.15 m into the ground and driven through a pre-drilled hole (300 mm diameter, 1.37 m deep). All piles were connected by a rigid cap that was not in contact with the ground surface. At the site, the soil profile consisted of sandy gravel (from the surface to 1.5 m), a hydraulic fill of clean sand (down to 12.2 m), and stiff silty clay interbedded with sand layers (down to 14.3 m) resting on bedrock. A dry unit weight of 15.7 kN/m^3, water content of 22.6%, and soil internal friction angle of 35.4° were reported by Briaud et al. (1989) for the hydraulic fill; a coefficient of horizontal pressure $K = 1.72$ and an interface friction angle equal to two-thirds of the soil friction angle were back-calculated for the pile group. The ground model in Fig. 4a was used for this analysis: five layers resting on a rigid base with a shear modulus of $G_3 = 38.3$ MPa for the sandy hydraulic fill, as suggested by Mandolini and Viggiani (1997) who interpreted the site investigation data, along with $\nu_s = 0.2$. A total capacity of $Q_t = 0.5$ MN is inferred from both the single pile and the pile group loading tests. These properties and ground model were also adopted for the COMPILE model analysis.

Fig. 4b compares the COMPILE load-settlement curves for the capped pile group for elastic EL and hyperbolic NP ($R_f = 1$) soil models against field measurements from Briaud et al. (1989) and with predictions obtained using the hyperbolic Boundary Element Method (BEM) (Mandolini and Viggiani, 1997) or Winkler models (Lee and Xiao, 2001) with a single pile, combined with pile-pile interaction factors. Importantly, COMPILE can replicate the elastic results from Mandolini and Viggiani (1997), giving the initial tangent stiffness of the pile group, while, because of its ability to replicate the soil stiffness degradation, it also agrees well with the field measurements up to large settlements. Notably, the proposed model predictions are slightly closer to the field data than the results given by the other approaches. Considering that COMPILE is more complex than the models by Mandolini and Viggiani (1997) and Lee and Xiao (2001), this agreement confirms its robustness.

5. Tunnel-single pile interaction: Uniform and layered ground

For the case of tunnelling, the proposed COMPILE model has been validated, against the PGROUPN BEM model of Basile (2014), for unloaded single piles in homogeneous ground with a perfectly-plastic EP behaviour (Franza et al., 2021). Thus, it is of interest for tunnelling analyses to consider the effects of layered ground conditions combined with non-linear soil-pile load transfer mechanisms. In this section, a loaded single pile (with constant head load) embedded in a two-layer ground is considered, as shown in Fig. 5a. This is identical to the ground model used by Huang and Mu (2012) in their linear elastic EL study. The analysis considers a pile in a two-layered ground with $L_p = 25$ m, $d_p = 0.8$ m, and $E_p = 30$ GPa that is affected by ground settlements induced by a 6 m diameter tunnel with a depth to axis level of 20 m, a horizontal offset from the tunnel centreline to the pile axis of 4.5 m, and a tunnel volume loss $V_{l,t} = 1\%$. Consistent with Huang and Mu (2012), greenfield movements were estimated with the formulas from Loganathan and Poulos (1998).

The ground considered is a two-layered half-space with a top layer thickness H of 10 m, a Poisson's ratio $\nu_s = 0.5$, and a range of Young's modulus of $E_{s,0}^{L,1} = 6-48$ MPa for the top layer and $E_{s,0}^{L,2} = 12-96$ MPa for the bottom layer. In particular, Fig. 5 reports results from a sensitivity study considering ratios between top and bottom layer stiffness of $E_{s,0}^{L,1}/E_{s,0}^{L,2} = 0.25$, 0.5, 1, and 2 with fixed $E_{s,0}^{L,1} = 24$ MPa; outcomes for a fixed bottom layer stiffness are provided as "Supplemental Materials". In the elastoplastic EP and nonlinear elastoplastic NP solutions, the ultimate base and shaft resistances were given by $q_f = 540$ kPa and $\tau_f = 48$ kPa (assumed constant along the pile), respectively, while a $SF_0 = 2$ was assumed. Note, however, that any distribution of τ_f along the pile can be implemented in the new modelling framework presented herein.

To validate the linear elastic EL model results for tunnel-single pile interaction in a layered ground, Fig. 5b compares COMPILE linear elastic EL results (settlements and axial forces within the pile; with positive settlements being downwards, and negative axial forces being compressive) against the results from Huang and Mu (2012). The agreement

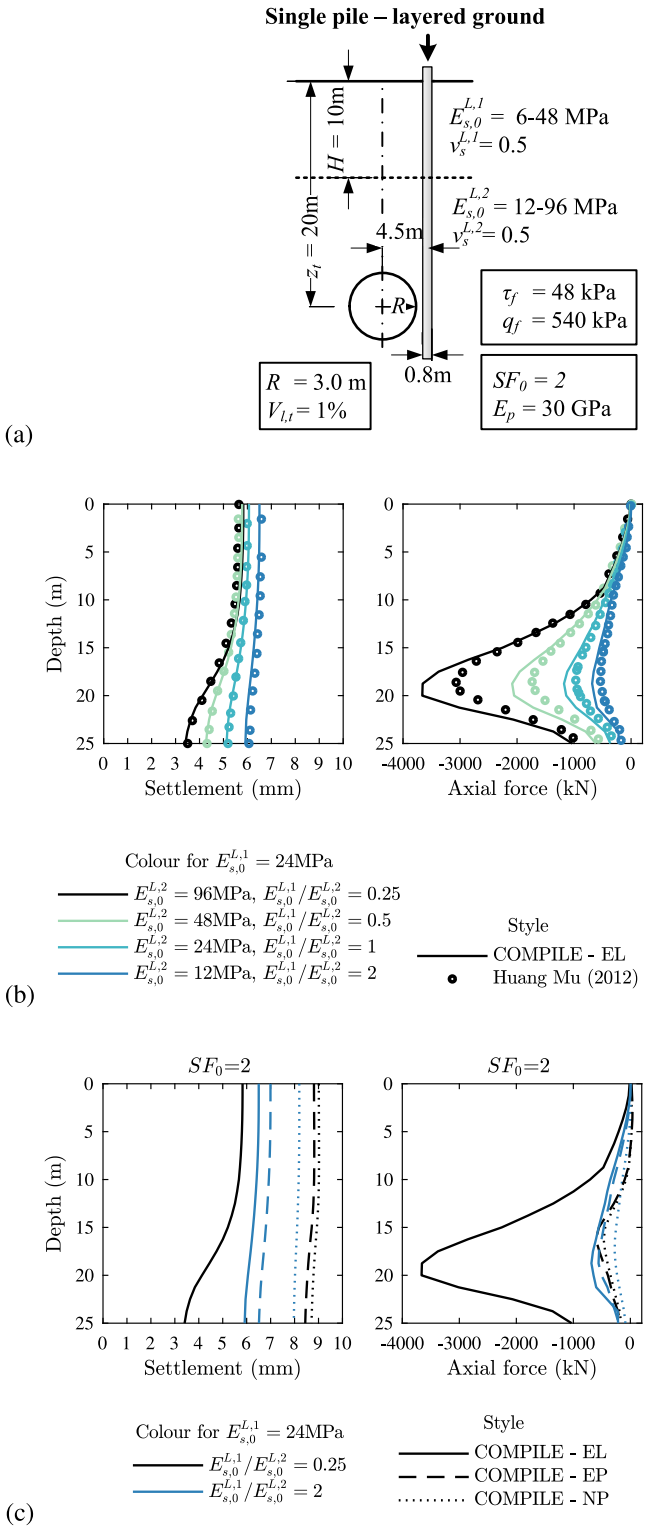

Fig. 5. (a) Studied single pile configuration in a layered ground; (b) tunnelling adjacent to a single pile in a layered ground: elastic validation analyses; (c) tunnelling adjacent to a single pile in a layered ground: the effects of soil behaviour.

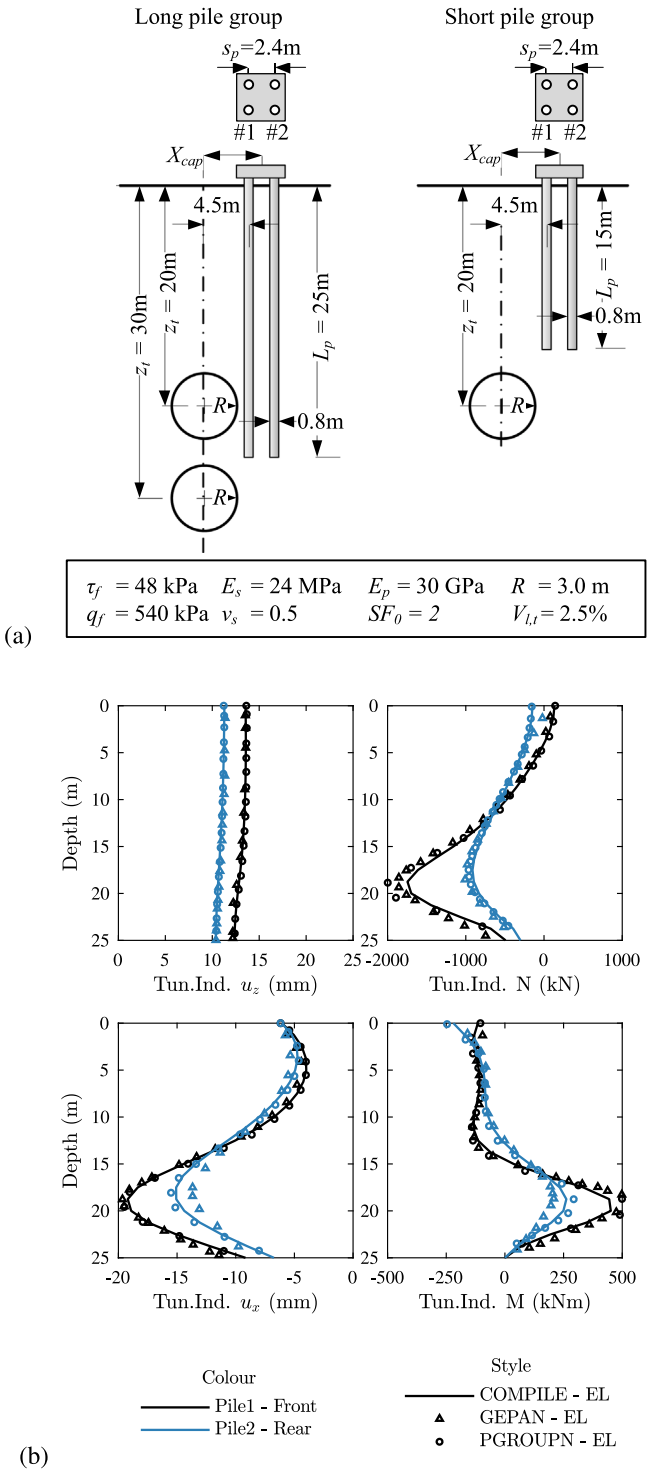

Fig. 6. (a) Scenarios considered for tunnelling near to capped 2x2 pile groups: 'long' piles and 'short' piles; (b) comparison of the elastic tunnelling-induced results for the 'long' pile group ($z_t = 20$ m; $L_P = 25$ m) against BEM predictions.

with the elastic results from Huang and Mu (2012) is good, particularly for settlements. As expected, decreasing the stiffness of the top layer (i.e. reducing $E^{L,1}_{s,0}/E^{L,2}_{s,0}$), which is associated with larger greenfield settlements, reduces the negative friction generated within the top layer. This decreases pile settlements and the magnitude of compressive axial forces. The largest value of the bottom layer stiffness $E^{L,2}_{s,0}$ = 96 MPa ($E^{L,1}_{s,0}/E^{L,2}_{s,0} = 0.25$ in Fig. 5b) gives the largest compressive axial force caused by the ground settlement (which in greenfield conditions reduces in magnitude with depth) due to the greater soil stiffness near the pile tip. On the other hand, reducing the bottom layer stiffness (i.e. increasing $E^{L,1}_{s,0}/E^{L,2}_{s,0}$) significantly reduces compressive forces of the pile together with slightly larger tunnelling-induced settlements.

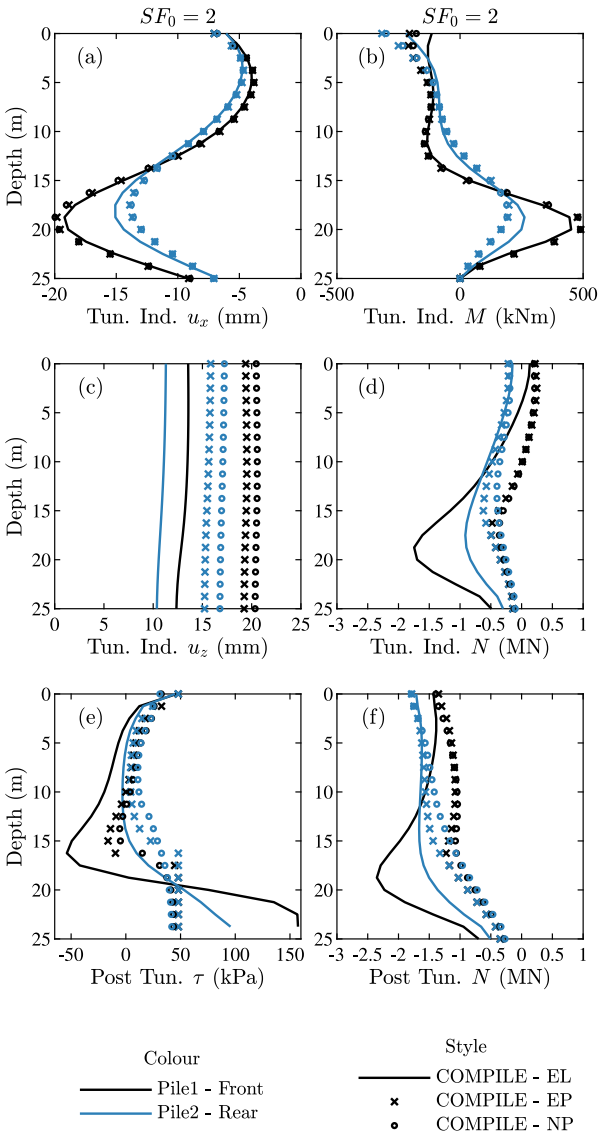

Fig. 7. Tunnelling adjacent to the 'long' pile group ($z_t = 20$ m; $L_P = 25$ m): initial safety factor $SF_0 = 2$.

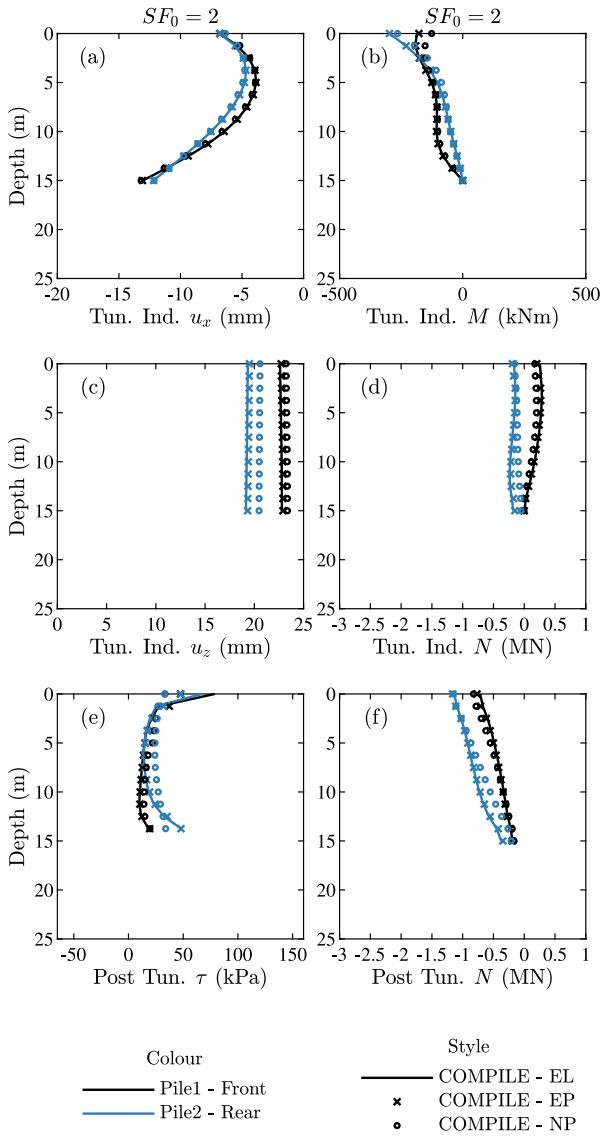

Fig. 8. Tunnelling beneath the 'short' pile group ($z_t = 20$ m; $L_P = 15$ m): initial safety factor $SF_0 = 2$.

The effects of more complex load-transfer mechanisms (i.e. using the EP and NP models) are considered in Fig. 5c. They show tunnelling-induced settlements and pile axial forces for selected layered ground conditions and for a (constant) head load P_0, giving an initial safety factor $SF_0 = Q_t/P_0 = 2$. For tunnelling adjacent to a pile, the EP and NP solutions increase settlements and considerably decrease axial forces compared to the EL results in qualitative agreement with Basile (2014) who considered a homogeneous soil. Fig. 5c also provides novel insights into the effects of stiffness degradation, with NP results further decreasing compressive forces and increasing tunnelling-induced settlements compared to the perfectly-plastic EP results. Finally, the impact of the ratio $E_{s,0}^{L,1}/E_{s,0}^{L,2}$ is most significant for the elastic (EL) case, and decreases when accounting for soil yielding (EP) and stiffness degradation (NP). Note that the tunnel-pile interaction for EP and NP near-pile behaviour also depends on both the tunnel volume loss $V_{l,t}$ and on the pile loading condition SF_0 (Basile, 2014; Franza et al., 2021), however a full parametric study of these parameters was considered beyond the scope of this paper.

6. Tunnel-pile group interaction: Rigid elevated caps

This section presents the response of 2 × 2 pile groups with a rigid elevated cap (i.e. no soil-pile cap contact) to adjacent and underlying tunnelling, analysing the ideal scenarios in Fig. 6a. The piles have diameter $d_p = 0.8$ m, a spacing of 2.4 m, and length L_p of either 15 m or 25 m, referred to as 'short' and 'long' piles, respectively; the Young's modulus of the piles was $E_p = 30$ GPa in all cases. The piles are embedded in homogeneous ground with a Young's modulus $E_{s,0} = 24$ MPa and a Poisson's ratio $\nu_s = 0.5$; the ultimate base and shaft resistances were set equal to $q_f = 540$ kPa and $\tau_f = 48$ kPa, while the pile external loads were adjusted to obtain initial safety factors of $SF_0 = 1.5, 2$, and 5, though the discussion here focuses on the $SF_0 = 2$ case. "Supplemental Materials" are provided for $SF_0 = 1.5$ and 5. The tunnel, with a radius of 3 m, has its centre located at a depth z_t of either 20 m or 30 m, with a horizontal offset from the closest pile axis of 4.5 m; a tunnel volume loss of $V_{l,t} = 2.5\%$ was considered. Greenfield movements were estimated using the semi-analytical expressions of Loganathan and Poulos (1998), similar to benchmark results from Loganathan et al. (2001) and Basile (2014). Pile 1 is the front pile closest to the tunnel and Pile 2 is the more distant rear pile.

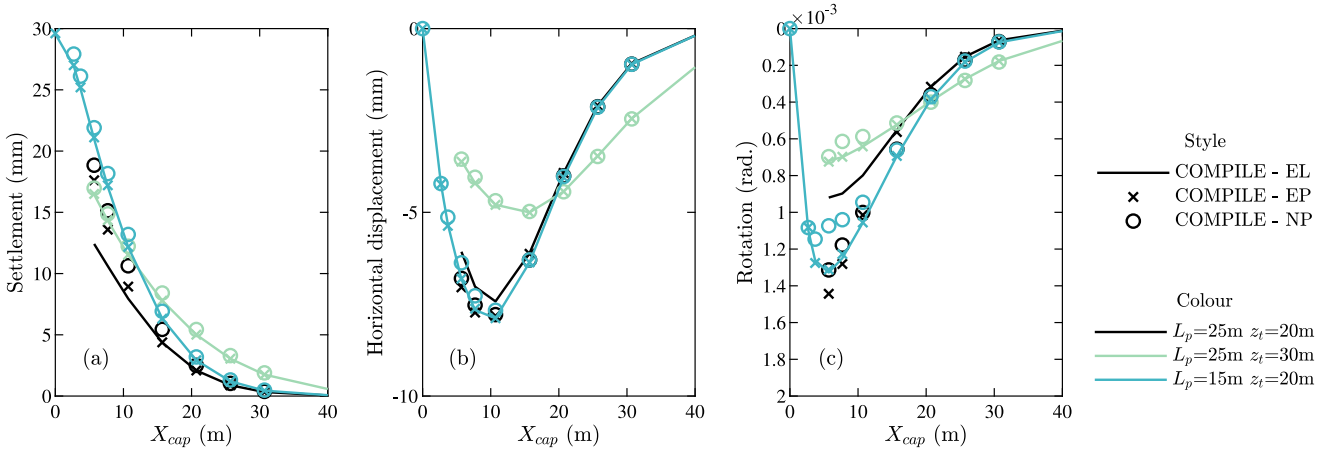

Fig. 9. Displacement of the cap for the 2x2 pile group with $SF_0 = 2$.

To investigate the response of pile groups to tunnelling, the elevated cap and pile group stiffness matrix, and the soil elastic flexibility matrix, are needed. For COMPILE, the elastic EL validation is presented first, by considering tunnel excavation adjacent to 'long' piles, as displayed in Fig. 6a. This configuration, with a tunnel at $z_t = 20$ m adjacent to the 'long' pile group, was also analysed elastically using the BEM by Loganathan et al. (2001) and Basile (2014), who developed models named GEPAN and PGROUPN, respectively. Fig. 6b illustrates a good match between COMPILE and the two BEM model results, agreeing particularly well with the PGROUPN results of axial forces and bending moments near the pile cap reported by Basile (2014). For the EL case, the relationship between pile cap displacements and tunnel-pile group offset (X_{cap} in Fig. 6a) predicted by COMPILE also agrees well with the GEPAN results, as reported by Franza et al. (2019).

Subsequently, COMPILE was used to evaluate the impact of soil yielding (EP) and of ground stiffness degradation (NP) when tunnelling beneath and adjacent to 'short' and 'long' pile groups. Fig. 7 displays the vertical and horizontal responses of piles with an initial safety factor $SF_0 = 2$ induced by the 'shallow' tunnel ($z_t = 20$ m) adjacent to the 'long' ($L_p = 25$ m) piles, whereas Fig. 8 presents such results for the 'shallow' tunnel beneath the 'short' ($L_p = 15$ m) piles. In particular, tunnelling-induced vertical u_z and horizontal u_x displacements, axial forces N, and bending moments M are reported; post-tunnelling axial forces and mobilised shaft friction τ are also included (depending on initial external loads and tunnelling effects). Post-tunnelling values of N can indicate the risk for tensile pile cracking, while mobilised shaft friction τ details the portion of soil along the pile that yields due to active and passive loads. This is important because, along with the tunnelling action, piles need to satisfy equilibrium by withstanding the pile head forces (applied by external loads and the superstructure).

Fig. 7 shows that for both the front pile 1 and the rear pile 2, the settlement u_z increases when nonlinear load transfer mechanisms EP and NP are considered for tunnelling adjacent to the 'long' piles. On the other hand, there is only a slight increase in pile settlement of the front pile 1 in Fig. 8 for tunnelling beneath the 'short' pile foundation. Also, the considered nonlinearities of shear stresses at the shaft and base force (in EP and NP models) have limited effects on pile horizontal movements u_x and on their bending moments M for both pile locations. Interestingly, bending moments at the pile heads are similar for 'long' and 'short' piles in Figs. 7b and 8b, due to the kinematic constraint applied by the stiff cap.

For tunnelling adjacent to the 'long' piles, the tunnelling-induced axial forces in Fig. 7d show that the soil yielding and non-linear behaviour limit the compressive (negative) forces at the tunnel springline depth ($z_t = 20$ m). This is due to the mobilisation of the full positive shaft friction below the tunnel axis (see the post-tunnelling τ in Fig. 7e), which also increases the pile settlement. In contrast, the axial forces along the rear pile 2 are similar for the EL and EP models, while the stiffness degradation within the NP model causes a minor decrease in the compressive forces close to the tunnel springline depth. For both piles 1 and 2, post-tunnelling axial forces are compressive along the entire pile in Fig. 7f. For the front pile 1 there is a tunnelling-induced shift in the axial forces towards tensile (positive) values near the pile head caused by the cap action. Regarding tunnelling beneath the shorter piles in Fig. 8, the soil yielding (EP) and stiffness degradation (NP) only alter the effects of tunnelling on pile axial forces slightly. "Supplemental Materials" are provided with results for $SF_0 = 1.5$ and 5.

Pile head and cap displacements are also of interest to enable the assessment of the impact of tunnelling on the superstructure, which may be a building or some other infrastructure. The tunnelling-induced cap displacements were analysed by varying the horizontal offset X_{cap} (refer to Fig. 6a) from the pile cap centre to the tunnel centreline. Results are displayed in Fig. 9 for the three scenarios depicted in Fig. 6a.

Comparison of results for 'long' piles ($L_p = 25$ m) with $z_t = 20$ m and $z_t = 30$ m indicates that the increase in tunnel depth influences the cap lateral displacement, decreases the maximum rotations obtained for the lower values of tunnel-pile group offset (i.e. X_{cap} lower than 15 m), and only increases the cap settlement slightly. Although tunnelling beneath piles is associated with greater potential for settlements than tunnelling adjacent to them, for a given pile length, the larger z_t needed to locate the tunnel beneath the piles results in smaller greenfield movements affecting the foundation; thus, there are two counteracting mechanisms associated with the increase in z_t. Regarding the near-pile soil model, cap horizontal displacements demonstrate a limited dependency on the soil nonlinearities (EP and NP), while the greatest increase in settlements are due to the soil yielding in the EP solution for tunnelling adjacent to the pile group. On the other hand, the soil stiffness degradation in NP analyses decreases the pile rotations (proportional to the front and rear pile differential settlement) with respect to the EL and EP models. Overall, elastic EL models are in good agreement with the EP predictions for tunnelling beneath the pile group, while there are minor differences with the nonlinear NP outcomes.

7. Tunnel-pile row interaction: Free pile-heads and stiff structures

When tunnelling in urban areas, engineers need to estimate the risk of damage and distortions within affected foundations and superstructures. In practice, risk assessments are mostly empirical and based on single piles with a free-head condition (Selemetas and Standing, 2017). Possible shortcoming of this approach are evaluated in this section

by analysing the response of piled structures to tunnelling using the proposed model.

The case of a tunnel beneath the centre of a building founded on a row of piles is considered, as illustrated in Fig. 10. The above-ground structure is either a concrete slab foundation with a flexible superstructure or a wall bearing masonry building with 4 or 7 storeys. These structures are modelled as an equivalent beam (respectively, $EI = 10, 216, 1158\,\mathrm{GNm}^2$) tied to the pile heads but not in contact with the soil. To distinguish between piles, they are labelled with numbers and with letters for the 5 and 11 pile rows, respectively (1 to 3 and A to F from the central to the external pile). On the other hand, tunnelling, ground, and pile conditions are identical to those of the 2 × 2 pile group in Fig. 6a, except that the tunnel is located centrally beneath the structure at a depth $z_t = 30\,\mathrm{m}$ and that the transverse pile spacing is 5 m. To isolate the effects of the building stiffness, the building weight is kept constant and was obtained for an initial safety factor $SF_0 = Q_t/P_0 = 2$, assuming that pre-tunnelling pile loads transferred from the structure are the same for all piles. To estimate the effects of the superstructure stiffness on the tunnel-pile-structure interaction, two types of analyses were performed: (1) free-head conditions with constant P_0 and (2) an active superstructure.

Fig. 11 displays the tunnelling-induced vertical u_z and horizontal u_x displacements (including surface greenfield GF values for reference), along with the post-tunnelling axial forces N and bending moments M predicted at the pile heads. In the case of free pile-heads, piles with an offset from the tunnel centreline lower than 10 m settled significantly more than the greenfield surface, while greenfield settlements are similar to pile vertical movements for the external piles with an offset greater than 10 m; this is in agreement with previous research (Selemetas and Standing, 2017). When the structure stiffness is activated, all models in Fig. 11 show a reduction of the settlement of piles 1 and A (i.e. the piles directly above the tunnel). This is due to the superstructure acting to unload the central piles and to transfer vertical loads towards the external piles. Interestingly, in Fig. 11, the greater the superstructure stiffness, the greater the decrease in the building distortion (quantified by the slope between pile head settlements); building distortions are reduced by both the restraining of the central piles and the embedment of the external piles. In particular, the NP solution indicates that the stiffest 7-storey building reduced its distortion with respect to the slab foundation (compare subplots b and d) by both driving the external piles downwards and uplifting the central piles; this is similar to the mechanism observed in centrifuge tests reported by Franza and Marshall (2018) and Song and Marshall (2020). Also, nonlinear hyperbolic NP solutions in Fig. 11 show greater settlements than the elastic EL and elastic perfectly-plastic EP solutions, particularly for the stiff building, although the vertical load redistribution described by pile head axial forces in Fig. 11 is lower for the NP model than for EL and EP models due to the soil stiffness degradation. However, building distortion levels are not highly affected by the soil behaviour (compare EL and NP trends). Note also that the largest pile head bending moments M are associated with the flexible slab, rather than with the stiff buildings, due to the larger slope of the settlement profiles, requiring greater pile head rotations. Finally, building distortions for the elastic (EL) and perfectly-plastic (EP) models are almost equal for all cases considered.

Subsequently, subsurface profiles of pile displacements and internal forces for the slab founded on the 5 pile row are plotted in Figs. 12 and 13, considering free pile-heads and an active structure, respectively. This case is used to demonstrate the interesting coupling that occurs between the bending and axial responses of external piles. The superstructure stiffness slightly increases the slope of the vertical profile of settlement u_z with depth for piles 1 and 3 in subplots a, resulting from the larger changes in axial forces imposed by the superstructure at the pile heads (confirmed by subplots c). These figures also confirm that, by 'activating' the structure, the settlements of the central pile 1 decrease, the embedment of the external pile 3 increases, and the differential

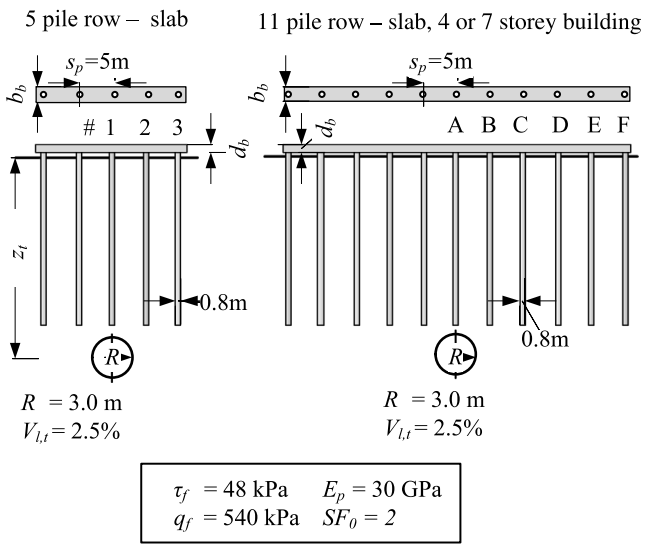

Fig. 10. Studied pile row configuration in homogeneous ground: (a) 5 and (b) 11 pile row foundation.

settlement between the central and external piles 1 and 3 (associated with superstructure distortions) decreases. Tunnelling-induced axial forces in subplots c show that tensile forces are generated by the subsurface ground settlements along both the central and intermediate piles 1 and 2, with the greatest tensile forces in the central pile 1. Importantly, accounting for soil plasticity and non-linearity in the EP and NP analyses (see Figs. 12 and 13) reduces tunnelling-induced axial forces for all piles (in terms of both compressive forces in the external pile 3 and tensile forces in the central pile 1), particularly for the free-head condition, contrary to the limited impact of soil nonlinearities on the building distortions (see Fig. 11).

To evaluate the pure axial pile distress, the pile that underwent the largest tensile tunnelling-induced axial force N is considered. Fig. 14 shows the vertical response of pile A for the 11-pile foundation (directly above the tunnel, see Fig. 10) and its dependency on the structure stiffness. In particular, the tunnelling-induced forces and displacements, as well as post-tunnelling axial forces and mobilised shaft friction, are displayed. Note that post-tunnelling forces can be related to the axial strains experienced by the pile, as $\varepsilon = N/E_pA_p$. The stiffest 7-storey building restrains the tunnelling-induced settlement by applying a variation in axial force at the pile head that propagates with depth by mobilising further positive shaft friction along the pile (see subplot d). As a consequence, in subplot c, post-tunnelling axial forces for the slab are positive only in the area near the pile tip, while the entire pile is subjected to tensile strains for the stiff 7-storey building. Soil behaviour also plays a role, with nonlinear stiffness degradation (NP) and yielding (EP) models providing smaller maximum pile axial tensile forces; in particular, the fact that no soil traction stresses can be applied at the pile base (a gap would form between the soil and the pile base) greatly affects the potential for post-tunnelling tensile (positive) axial forces.

8. Capacity envelopes for pile assessment

It is common to evaluate the risk for pile damage by predicting excavation-induced tensile forces and bending moments (often from single pile analyses with free pile-heads) and comparing their values against limit thresholds (Loganathan et al., 2001). However, this approach has limitations: post-tunnelling internal forces should be used (Franza et al., 2021); the free pile-head approach can be unconservative (as illustrated in the previous section); and allowable axial force-bending moment combinations should be used for structural assessments. Therefore, it is recommended, when possible, to estimate

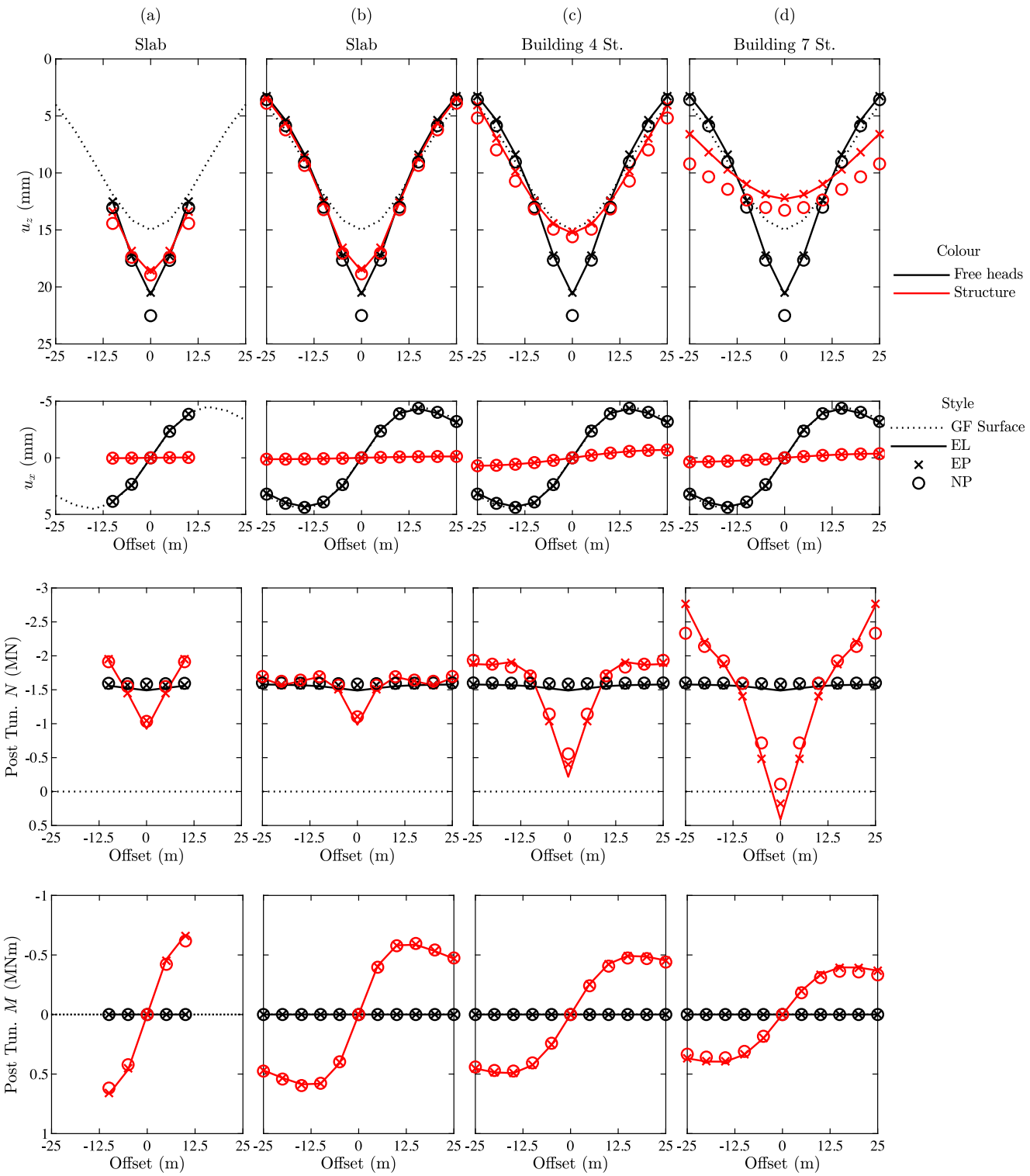

Fig. 11. Tunnelling-induced settlements (u_z), horizontal movements (u_x), post-tunnelling axial force (N) and bending moment (M) of the pile heads of piled structures: (a) 5 pile and (b) 11 pile row with slab; (c) 4 and (d) 7 storey building founded on 11 pile row.

post-tunnelling pile internal forces from coupled soil-pile-structure interaction analyses and, subsequently, to assess pile integrity by comparing their cross-sectional $N - M$ values against their cross-sectional *"capacity envelopes"*, where the allowable cross-sectional bending moment is a function of the pile characteristics (materials, cross-section, reinforcement, etc.) and of the local axial force acting at such cross-sections (e.g. the maximum tensile axial force is decreased by the presence of bending).

In this work, pile ultimate capacity envelopes are computed from the closed-form (simplified) formulas of Cosenza et al. (2011) for circular cross-sections (assuming a stress block ultimate behaviour for concrete, fully yielded steel, and rebar distributed as an equivalent ring), although any approach/software may be used to estimate the capacity envelopes (Di Laora et al., 2020). Using these formulas, the capacity envelope is a function of the pile diameter d_p, percentage ρ of steel reinforcement area within the total cross-section, rebar cover c,

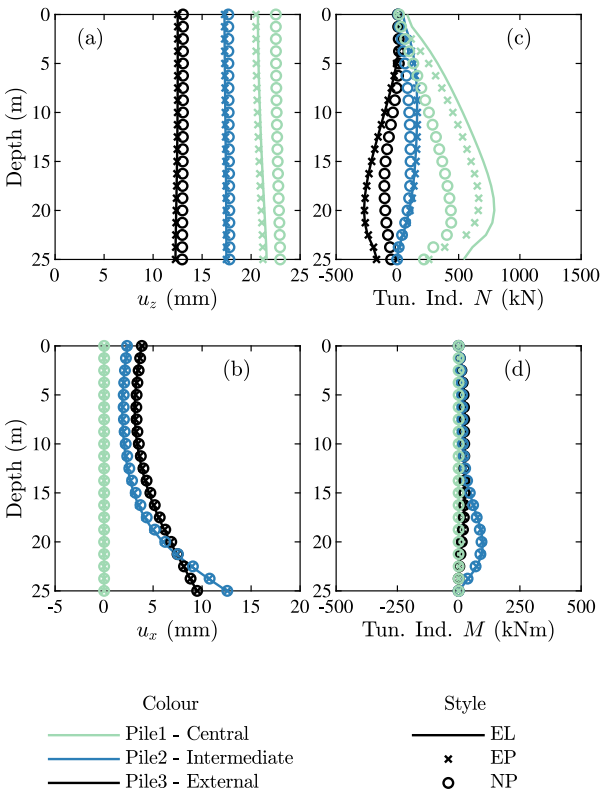

Fig. 12. Pile response to tunnelling beneath the 5-pile row: free pile-heads.

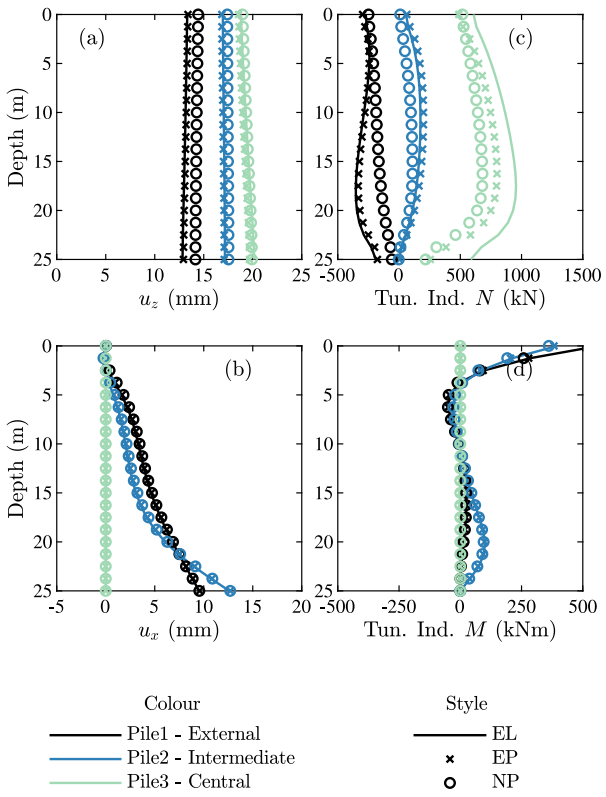

Fig. 13. Pile response to tunnelling beneath the 5-pile row: active slab.

and the design strength for concrete f_{cd} and steel f_{yd}. For the concrete piles of the structures in Fig. 10, it was assumed that $f_{cd} = 14$ MPa, $f_{yd} = 391$ MPa, $d_p = 0.8$ m, $c = 45$ mm, and $\rho = 0$ or 1% for either unreinforced (UC) or reinforced concrete (RC), respectively, which are common in urban areas.

Fig. 15 presents, as $N - M$ charts, the internal forces inferred at each pile from the analyses depicted in Fig. 10, along with capacity envelopes for UC and RC material. Regarding pure axial structural failure obtained along the abscissa-axis, Fig. 15 shows that, for all structures, a tensile (positive) axial force is induced (at piles 1 and A), both for free-heads and active structures. Free-head piles underwent tunnelling-induced tensile forces close to the tip where pre-tunnelling compression is low (see subplots a-d), whereas the greatest tensile forces are induced by the action of the stiffest 7-storey building (see subplot d). These tensile forces would likely fail the UC piles, while they could be accommodated by the RC piles.

Pile structural failure due to combined bending and axial internal forces should also be considered. For this, the role of the superstructure action is notable. The structure stiffness produces tunnelling-induced bending moments at the pile heads, while pile bending moments for free-head cases are limited. This is because the beam axial stiffness restrains the differential horizontal displacements of the pile heads (see Figs. 12b and 13b), and the pile reacts against the beam rotation caused by vertical deflection of the structure (see Figs. 13b and 13d). Interestingly, the UC piles beneath the relatively flexible slab (for both the 5 and 11 pile rows) experience the largest bending moments at the external piles, due to the greater slope of the slab deflection. On the other hand, the (relatively stiff) multi-storey buildings cause smaller bending moments than the slab, due to the lower building distortion slope. In addition, the external piles are more compressed by the multi-storey building, moving the $N-M$ data points towards the region with greater flexural capacity. Flexural distress at the pile heads would be critical for UC piles supporting the semi-flexible slab while, for all the analysed scenarios, RC piles would be resilient.

9. Conclusions

A new continuum-based model for soil-pile-structure interaction (COMPILE), capable of accounting for non-linear load transfer mechanisms (due to local yielding and stiffness degradation) and layered ground conditions, was proposed. The model can analyse single piles, pile groups, and piled structures (with stiff superstructures) affected by vertical loads and it can also analyse tunnelling-induced effects; predictions of pile settlements and deflections, internal forces and moments, and mobilised soil resistances along the pile shaft and base were illustrated. Results indicated that, for rational design and risk assessment purposes, interaction analyses that account for layered ground conditions and for the effect of a superstructure connecting pile heads are needed; free-head single pile analyses may be insufficient. The following specific conclusions may be drawn from the paper.

- The COMPILE model can reliably predict deep foundation response to vertical loads, as shown by comparison with field data and (simpler) non-linear models.
- For tunnelling adjacent to single piles and to pile groups, accounting for the limit forces at the shaft and base, and for the soil stiffness degradation, provides more realistic predictions of tunnelling-induced pile forces (i.e., variation of compressive axial force) and settlements, which also depend on greenfield movement magnitude and pre-tunnelling loads. Layered ground conditions play a role in the tunnel-pile-structure interaction, the nature of which depends on the type of load-transfer mechanism adopted for the soil-pile interface; engineering judgement is therefore needed when applying lessons from previous studies on tunnel-pile interactions in uniform soil to real cases with layered grounds.
- When tunnelling beneath piles, the considered scenarios presented a limited sensitivity (lower than for adjacent tunnelling) of

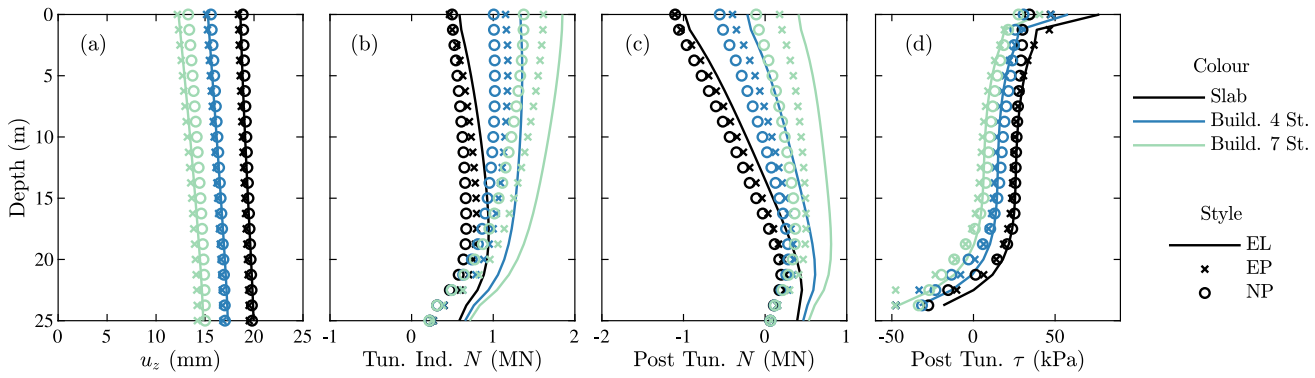

Fig. 14. Behaviour of the (central) pile directly above the tunnel in the 11 pile row interaction analysis: (a) tunnelling-induced settlements; (b) tunnelling-induced axial force variation; final (post-tunnelling) (c) axial force and (d) mobilised shaft friction profile.

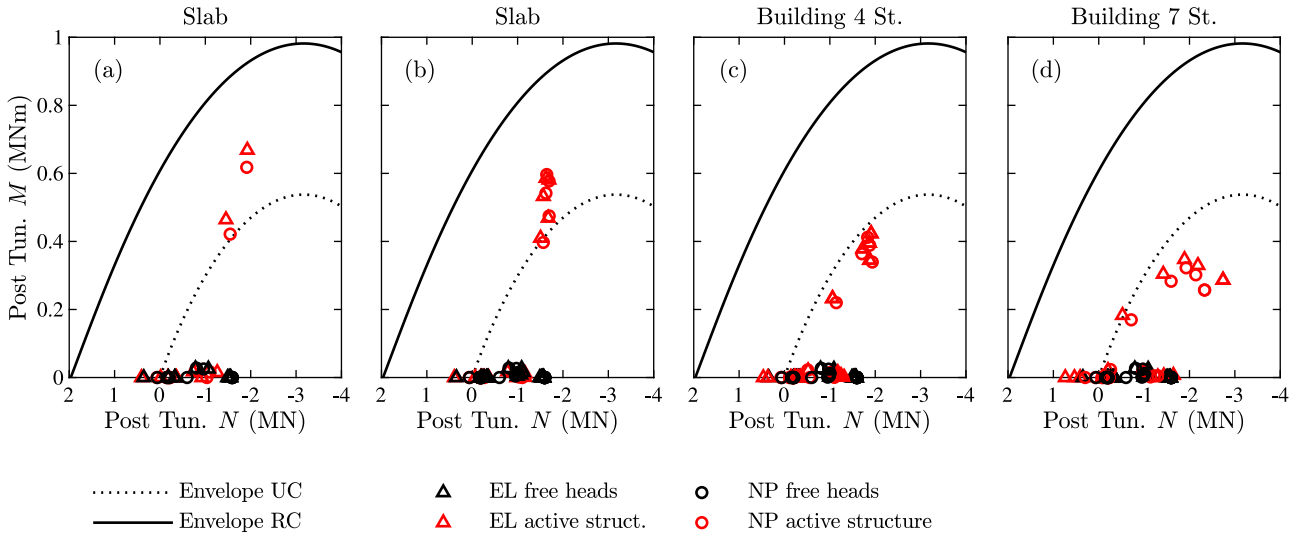

Fig. 15. Internal forces compared with limit envelopes for unreinforced (UC) and reinforced (RC) concrete piles: (a) 5 pile and (b) 11 pile row with slab; (c) 4 and (d) 7 storey building founded on 11 pile row.

the pile foundation displacements and forces to the adopted load-transfer mechanism, with possible post-tunnelling tensile forces developing in the pile directly above the tunnel. However, for stiff superstructures, the hyperbolic model predicted a slight increase in the settlement level compared to the elastic or perfectly-plastic analyses.

- For the analysed capped pile groups, the tunnelling-induced movements of the cap depended on counteracting interaction mechanisms when increasing the tunnel depth. Thus, considering the complexity of the problem, preliminary interaction analyses should be carried out, instead of applying greenfield displacements to the cap.
- The action of slabs and stiff superstructures decreases the distortions of the structure above ground, whereas it likely increases the foundation distress due to tunnelling. In particular, the actions applied at the pile heads by connected slabs, caps, or buildings may lead to the pile structural failure, which should be evaluated in terms of combined post-tunnelling axial and bending distress. Thus, free pile-head analyses may result in either conservative or unconservative risk assessments, depending on the risk criterion considered (e.g., settlement, pile structural failure, building distortion level). Also, soil-pile-structure interaction analyses indicated that semi-flexible structures could lead to tunnelling-induced pile bending forces that are greater than those associated with stiff buildings or free pile heads; this indicates that developing design envelopes based on fully-flexible and perfectly rigid superstructures will not always be conservative. As a result, soil-pile-structure interaction models are recommended for design.

The proposed model allows generic ground movement inputs; therefore, its application could be extended to a variety of static and pseudo-static soil-structure interaction problems. However, its practical limitations should be noted; the model is fully suitable for bored (non-displacement) piles, whereas driven/jacked (displacement) piles can currently only be considered in terms of pre-excavation load sequence in two-stage models, as indicated by Franza et al. (2021). Future work should attempt to evaluate the model's applicability to displacement piles and implement a soil-pile load transfer mechanism with a greater level of fidelity for this scenario.

CRediT authorship contribution statement

A. Franza: Conceptualization, Methodology, Software, Formal analysis, Data curation, Writing – original draft, Visualization, Funding acquisition. **C. Zheng:** Methodology, Software, Formal analysis, Writing – review & editing. **A.M. Marshall:** Conceptualization, Writing – review & editing. **R. Jimenez:** Conceptualization, Writing – review & editing, Supervision, Funding acquisition.

Declaration of competing interest

The authors declare that they have no known competing financial interests or personal relationships that could have appeared to influence the work reported in this paper.

Acknowledgements

This project has received funding from the European Union's Horizon 2020 research and innovation programme under the Marie Sklodowska-Curie grant agreement No 793715. Partial support was also provided by the Spanish Ministry of Science and Innovation, under Grant PID2019-108060RB-I00.

Appendix A. Supplementary data

Supplementary material related to this article can be found online at https://doi.org/10.1016/j.compgeo.2021.104386.

References

Ai, Z., Yue, Z., Tham, L., Yang, M., 2002. Extended Sneddon and Muki solutions for multilayered elastic materials. Internat. J. Engrg. Sci. 40 (13), 1453–1483. http://dx.doi.org/10.1016/S0020-7225(02)00022-8.

Basile, F., 1999. Non-linear analysis of pile groups. Proc. Inst. Civil Eng.- Geotech. Eng. 137 (2), 105–115. http://dx.doi.org/10.1680/gt.1999.370205.

Basile, F., 2014. Effects of tunnelling on pile foundations. Soils Found. 54 (3), 280–295. http://dx.doi.org/10.1016/j.sandf.2014.04.004.

Bel, J., Branque, D., Wong, H., Viggiani, G., Losacco, N., 2016. Impact of tunneling on pile structures above the tunnel: Experimental study on a 1g reduced scale model of TBM. In: ITA-AITES World Tunnel Congress 2016, Vol. 4. WTC 2016. pp. 3219–3229.

Briaud, J.L., Tucker, L.M., Ng, E., 1989. Axially loaded 5 pile group and single pile in sand. In: Proceedings of 12th International Conference on Soil Mechanics and Foundation Engineering, Vol. 2. Rio de Janeiro, Brazil. pp. 1121–1124.

Cairo, R., Conte, E., 2006. Settlement analysis of pile groups in layered soils. Can. Geotech. J. 43 (8), 788–801. http://dx.doi.org/10.1139/t06-038.

Castelli, F., Maugeri, M., 2002. Simplified nonlinear analysis for settlement prediction of pile groups. J. Geotech. Geoenviron. Eng. 128 (1), 76–84. http://dx.doi.org/10.1061/(ASCE)1090-0241(2002)128:1(76).

Chow, Y.K., 1986. Analysis of vertically loaded pile groups. Int. J. Numer. Anal. Methods Geomech. 10 (1), 59–72. http://dx.doi.org/10.1002/nag.1610100105.

Cosenza, E., Galasso, C., Maddaloni, G., 2011. A simplified method for flexural capacity assessment of circular RC cross-sections. Eng. Struct. 33 (3), 942–946. http://dx.doi.org/10.1016/j.engstruct.2010.12.015.

Di Laora, R., Galasso, C., Mylonakis, G., Cosenza, E., 2020. A simple method for N-M interaction diagrams of circular reinforced concrete cross sections. Struct. Concr. 21 (1), 48–55. http://dx.doi.org/10.1002/suco.201900139.

Dias, T., Bezuijen, A., 2018a. Pile tunnel interaction: Pile settlement vs Ground settlements. In: ITA World Tunnel Congress 2018 - the Role of Underground Space in Building Future Sustainable Cities. Dubai, United Arab Emirates.

Dias, T.G.S., Bezuijen, A., 2018b. Load-transfer method for piles under axial loading and unloading. J. Geotech. Geoenviron. Eng. 144 (1), 04017096. http://dx.doi.org/10.1061/(ASCE)GT.1943-5606.0001808.

Franza, A., Marshall, A.M., 2018. Centrifuge modeling study of the response of piled structures to tunneling. J. Geotech. Geoenviron. Eng. 144 (2), 04017109. http://dx.doi.org/10.1061/(ASCE)GT.1943-5606.0001751.

Franza, A., Marshall, A.M., Haji, T., Abdelatif, A.O., Carbonari, S., Morici, M., 2017. A simplified elastic analysis of tunnel-piled structure interaction. Tunn. Undergr. Space Technol. 61, 104–121. http://dx.doi.org/10.1016/j.tust.2016.09.008.

Franza, A., Marshall, A.M., Jimenez, R., 2019. Elastic analysis of tunnelling beneath capped pile groups. In: Sigursteinsson, H., Erlingsson, S., Bessason, B. (Eds.), Proceedings of the XVII ECSMGE-2019: Geotechnical Engineering Foundation of the Future. Icelandic Geotechnical Society, Reykjavík, Iceland, http://dx.doi.org/10.32075/17ECSMGE-2019-0529.

Franza, A., Marshall, A.M., Jimenez, R., 2021. Non-linear soil-pile interaction induced by ground settlements: pile displacements and internal forces. Géotechnique 71 (3), 239–249. http://dx.doi.org/10.1680/jgeot.19.P.078.

Franza, A., Sheil, B., 2021. Pile groups under vertical and inclined eccentric loads: elastoplastic modelling for performance based design. Comput. Geotech. 135, 104092. http://dx.doi.org/10.1016/j.compgeo.2021.104092.

Hong, Y., Soomro, M., Ng, C., 2015. Settlement and load transfer mechanism of pile group due to side-by-side twin tunnelling. Comput. Geotech. 64, 105–119. http://dx.doi.org/10.1016/j.compgeo.2014.10.007.

Huang, M., Mu, L., 2012. Vertical response of pile raft foundations subjected to tunneling-induced ground movements in layered soil. Int. J. Numer. Anal. Methods Geomech. 36 (8), 977–1001. http://dx.doi.org/10.1002/nag.1035.

Korff, M., Mair, R.J., Tol, F.A.F.V., 2016. Pile-soil interaction and settlement effects induced by deep excavations. J. Geotech. Geoenviron. Eng. 142 (8), 04016034.

Lee, K.M., Xiao, Z.R., 2001. A simplified nonlinear approach for pile group settlement analysis in multilayered soils. Can. Geotech. J. 38 (5), 1063–1080. http://dx.doi.org/10.1139/t01-034.

Leung, Y.F., Klar, A., Soga, K., 2010. Theoretical study on pile length optimization of pile groups and piled rafts. J. Geotech. Geoenviron. Eng. 136 (2), 319–330. http://dx.doi.org/10.1061/(ASCE)GT.1943-5606.0000206.

Liu, J., Xiao, H., Tang, J., Li, Q., 2004. Analysis of load-transfer of single pile in layered soil. Comput. Geotech. 31 (2), 127–135. http://dx.doi.org/10.1016/j.compgeo.2004.01.001.

Loganathan, N., Poulos, H.G., 1998. Analytical prediction for tunneling-induced ground movements in clays. J. Geotech. Geoenviron. Eng. 124 (9), 846–856. http://dx.doi.org/10.1061/(ASCE)1090-0241(1998)124:9(846).

Loganathan, N., Poulos, H.G., Xu, K.J., 2001. Ground and pile-group responses due to tunnelling. Soils Found. 41 (1), 57–67.

Mandolini, A., Viggiani, C., 1997. Settlement of piled foundations. Géotechnique 47 (4), 791–816. http://dx.doi.org/10.1680/geot.1997.47.4.791.

Marshall, A.M., Franza, A., Jacobsz, S.W., 2020. Assessment of the posttunneling safety factor of piles under drained soil conditions. J. Geotech. Geoenviron. Eng. 146 (9), 04020097. http://dx.doi.org/10.1061/(ASCE)GT.1943-5606.0002348.

Marshall, A.M.A., Mair, R.R.J., 2011. Tunneling beneath driven or jacked end-bearing piles in sand. Can. Geotech. J. 48 (12), 1757–1771. http://dx.doi.org/10.1139/t11-067.

Mindlin, R.D., 1936. Force at a point in the interior of a semi-infinite solid. J. Appl. Phys. 7 (5), 195–202. http://dx.doi.org/10.1063/1.1745385.

Mu, L., Huang, M., Finno, R.J., 2012. Tunnelling effects on lateral behavior of pile rafts in layered soil. Tunn. Undergr. Space Technol. 28, 192–201. http://dx.doi.org/10.1016/j.tust.2011.10.010.

Ng, C., Soomro, M., Hong, Y., 2014. Three-dimensional centrifuge modelling of pile group responses to side-by-side twin tunnelling. Tunn. Undergr. Space Technol. 43, 350–361. http://dx.doi.org/10.1016/j.tust.2014.05.002.

O'Neill, M.W., Hawkins, R.A., Mahar, L.J., 1982. Load transfer mechanisms in piles and pile groups. J. Geotech. Eng. Div. 108 (12), 1605–1623.

Poulos, H.G., 1989. Pile behaviour - theory and application. Géotechnique 39 (3), 365–415.

Randolph, M.F., Wroth, C.P., 1979. Analytical solution for the consolidation around a driven pile. Int. J. Numer. Anal. Methods Geomech. 3 (3), 217–229.

Selemetas, D., Standing, J.R., 2017. Response of full-scale piles to EPBM tunnelling in London clay. Géotechnique 67 (9), 823–836. http://dx.doi.org/10.1680/jgeot.SIP17.P.126.

Sheil, B.B., McCabe, B.A., Comodromos, E.M., Lehane, B.M., 2019. Pile groups under axial loading: an appraisal of simplified non-linear prediction models. Géotechnique 69 (7), 565–579. http://dx.doi.org/10.1680/jgeot.17.r.040.

Song, G., Marshall, A.M., 2020. Centrifuge study on the influence of tunnel excavation on piles in sand. J. Geotech. Geoenviron. Eng. 146 (12), 04020129. http://dx.doi.org/10.1061/(ASCE)GT.1943-5606.0002401.

Soomro, M.A., Hong, Y., Ng, C.W.W., Lu, H., Peng, S., 2015. Load transfer mechanism in pile group due to single tunnel advancement in stiff clay. Tunn. Undergr. Space Technol. 45, 63–72. http://dx.doi.org/10.1016/j.tust.2014.08.001.

Stutz, H., Wuttke, F., Benz, T., 2014. Extended zero-thickness interface element for accurate soil-pile interaction modelling. In: Hicks, M.A., Brinkgreve, R.B.J., Rohe, A. (Eds.), Proceedings of the 8th European Conference on Numerical Methods in Geotechnical Engineering. NUMGE 2014, CRC Press/Taylor, Delft, Holland, pp. 283–288.

Williamson, M.G., Mair, R.J., Devriendt, M.D., Elshafie, M.Z.E.B., 2017. Open-face tunnelling effects on non-displacement piles in clay - part 2: tunnelling beneath loaded piles and analytical modelling. Géotechnique 67 (11), 1001–1019. http://dx.doi.org/10.1680/jgeot.SIP17.P.120.

Xu, K.J., Poulos, H.G., 2001. 3-D elastic analysis of vertical piles subjected to "passive" loadings. Comput. Geotech. 28 (2001), 349–375.

Yoo, C., 2013. Interaction between tunneling and bridge foundation - A 3D numerical investigation. Comput. Geotech. 49, 70–78. http://dx.doi.org/10.1016/j.compgeo.2012.11.005.

Zhang, Q.-q., Liu, S.-w., Zhang, S.-m., Zhang, J., Wang, K., 2016. Simplified non-linear approaches for response of a single pile and pile groups considering progressive deformation of pile-soil system. Soils Found. 56 (3), 473–484. http://dx.doi.org/10.1016/j.sandf.2016.04.013.

Zhang, Q.-Q., Zhang, Z.-M., He, J.-Y., 2010. A simplified approach for settlement analysis of single pile and pile groups considering interaction between identical piles in multilayered soils. Comput. Geotech. 37 (7–8), 969–976. http://dx.doi.org/10.1016/j.compgeo.2010.08.003.